Physics of Fluids

Newtonian and viscoelastic fluid flows through an abrupt 1:4 expansion with slip boundary conditions

Cite as: Phys. Fluids **32**, 043103 (2020); https://doi.org/10.1063/1.5145092
Submitted: 15 January 2020 . Accepted: 25 March 2020 . Published Online: 24 April 2020

L. L. Ferrás, A. M. Afonso, M. A. Alves, J. M. Nóbrega, and F. T. Pinho

Physics of Fluids ARTICLE scitation.org/journal/phf

Newtonian and viscoelastic fluid flows through an abrupt 1:4 expansion with slip boundary conditions

Cite as: Phys. Fluids 32, 043103 (2020); doi: 10.1063/1.5145092
Submitted: 15 January 2020 • Accepted: 25 March 2020 •
Published Online: 24 April 2020

L. L. Ferrás,[1,a] A. M. Afonso,[2,b] M. A. Alves,[3,b] J. M. Nóbrega,[4,b] and F. T. Pinho[2,b]

AFFILIATIONS

[1]CMAT—Centro de Matemática e Departamento de Matemática, Universidade do Minho, Campus de Azurém, 4800-058 Guimarães, Portugal
[2]Centro de Estudos de Fenómenos de Transporte, Departamento de Engenharia Mecânica, Faculdade de Engenharia da Universidade do Porto, Rua Dr. Roberto Frias s/n, 4200-465 Porto, Portugal
[3]Centro de Estudos de Fenómenos de Transporte, Departamento de Engenharia Química, Faculdade de Engenharia da Universidade do Porto, Rua Dr. Roberto Frias s/n, 4200-465 Porto, Portugal
[4]Institute for Polymers and Composites, University of Minho, Campus de Azurém, 4800-058 Guimarães, Portugal

[a]**Author to whom correspondence should be addressed:** luislimafr@gmail.com
[b]**Electronic addresses:** aafonso@fe.up.pt; mmalves@fe.up.pt; mnobrega@dep.uminho.pt; and fpinho@fe.up.pt

ABSTRACT

In this work, we present a systematic numerical investigation of the 1:4 planar expansion creeping flow under the influence of slip boundary conditions for Newtonian and viscoelastic fluids, the latter modeled by the simplified Phan–Thien–Tanner constitutive model. The linear and nonlinear Navier slip laws were considered with the dimensionless slip coefficient k_l^* varying in the range [0, 4500] and the slip exponents $m = 0.5$, 1, and 2. The simulations were carried out for a low Reynolds number, $Re = 0.001$, and for Deborah numbers (De) between 0 and 100. Convergence could not be achieved for higher values of the Deborah number and large values of the slip coefficient due to the large stress gradients near the singularity point (reentrant corner). The results obtained allow us to conclude that for all De, the increase in slip velocity leads to vortex suppression. The flow characteristics are described in detail for low values of the Deborah number, $De \leq 5$, while for higher De the main features are only shown for specific values of the slip coefficient. These results find application in polymer processing, where the use of lubricants that migrate to the wall is common, which promotes slip.

I. INTRODUCTION

The incompressible laminar flow in a symmetric plane sudden expansion is an interesting benchmark problem. Although the geometry is rather simple, the resulting flows are dynamically complex, depending on several factors such as the inlet boundary conditions, the Reynolds (Re) and Deborah (De) numbers, and the expansion ratio. This geometry is found in several industrial processes, such as in injection molding of polymer melts. Aiming to better understand this problem, several studies have been done, leading to new results and improved knowledge of the expansion flow dynamics for both Newtonian and non-Newtonian fluids, as described in the following.

Halmos and co-workers[1–3] presented experimental and numerical studies of flows of polymer solutions and polymer melts through an abrupt expansion, considering non-Newtonian inelastic and elastic constitutive models. They found good agreement between the experimental data obtained for polymers melts and the numerical simulations performed with a power-law model, but they used coarse meshes and low order discretization schemes. Townsend and Walters[4] and Baloch *et al.*[5] both used the Phan–Thien–Tanner (PTT) model[6] to compare their numerical results with the experimental results provided by Walters.[4] In all these studies, the conclusions were unanimous: viscoelasticity suppresses the secondary flows that appear at the salient corner, and this is justified with some kind of *swell* phenomenon that occurs to the main flow upon

transition to the larger channel (the fluid releases some of the stored energy resulting in the expansion of the main flow and the compression of the recirculation region). More recently, Poole *et al.*[7] investigated numerically the two-dimensional 1:3 expansion flow for fluids obeying the upper-convected Maxwell (UCM), Oldroyd-B, and PTT constitutive models. They found that the previous results published in the literature by Darwish *et al.*[8] and Missirlis *et al.*[9] were only qualitatively correct because of the poor mesh refinement used. In the work of Poole *et al.*,[7] the degree of recirculation suppression was shown to be much weaker than that suggested previously, and at high Deborah number flows, a significant recirculation region still exists.

The study of flow bifurcations in fluid mechanics has also received considerable attention as it enables better understanding of the problems of stability and transition to turbulent flow. For this specific topic, experimental results are given in the works of Durst *et al.*,[10] Cherdron *et al.*,[11] and Ouwa *et al.*,[12] whereas numerical predictions, as well as a good review of the literature regarding the bifurcation phenomena for Newtonian and non-Newtonian fluids, can be found in the work of Wahba.[13]

For the bifurcation phenomenon in viscoelastic fluids, we highlight the work of Rocha *et al.*,[14] where a numerical investigation of viscoelastic flows (FENE–CR constitutive model) through a planar 1:4 sudden expansion is presented. They found that viscoelasticity stabilizes the laminar flow under conditions of non-negligible inertia and results in symmetric flow patterns up to a Reynolds number of about 46. Poole *et al.*[15] arrived at similar conclusions based on laminar flow experiments with a viscoelastic liquid through a symmetrical plane sudden expansion preceded by a gradual contraction from a square duct. Therefore, since creeping flow conditions are employed in this work, and based on the symmetric expansion flows obtained by Poole *et al.*,[7] we assume the existence of flow symmetry relative to the flow centerline.

For turbulent flows, more information can be found in the experimental work of Abbott and Kline,[16] about the subsonic turbulent flow over single and double backward facing steps, and the experimental works of Escudier *et al.*,[17] Poole *et al.*,[18,19] and Dales *et al.*[20]

The interested readers can also consult the papers on slip velocity and expansion flows.[21–30]

All the previous works concerned either Newtonian or non-Newtonian inelastic and viscoelastic fluids. The viscoelastic fluids usually present a more complex rheological and dynamic behavior, when compared to Newtonian fluids, and one of these complex features is the ability of the fluid to show some degree of slip[31–40] along the wall, found in some polymer melt flows. However, in the literature, we could not find the influence of slip boundary conditions on the fluid flow behavior through an abrupt expansion, and this feature is very important in polymer processing, where contraction and expansion flows are often encountered.

For this reason, this work presents a numerical study looking at the influence of slip velocity (considering both linear and nonlinear Navier slip boundary conditions) on the flow through an abrupt 1:4 expansion (see Fig. 1), for $Re = \rho U_1 H_1/\eta_0 = 0.001$ and a wide range of dimensionless linear slip coefficients $k_l^* = \frac{k\eta_0}{H_1} \in [0, 4500]$ and Deborah numbers, $De = \lambda U_1/H_1 \in \{0, 1, 2, 3, 4, 5, 10, 50, 100\}$. These dimensionless numbers are defined based on the inlet velocity,

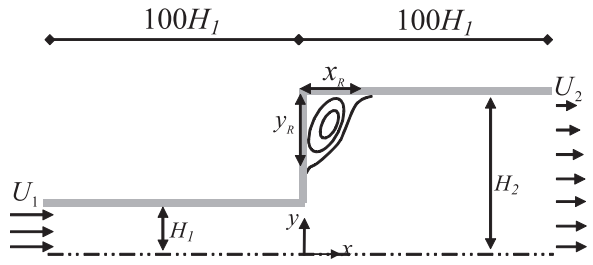

FIG. 1. Schematic of the 1:4 expansion geometry. U_1 and U_2 represent the average inlet and outlet velocities, respectively, and H_1 and H_2 represent the inlet and outlet half width.

U_1, and entrance half width, H_1, with ρ and λ being the density and relaxation time of the viscoelastic fluid and η_0 being the sum of polymer and solvent zero-shear viscosities. k represents a slip length (the subscript l in k_l^* stands for the linear slip model, to be defined later). We study both Newtonian and non-Newtonian fluids modeled by the simplified PTT (sPTT) model, and we present a detailed study on the flow characteristics such as the influence of the slip velocity on the vortex size, vortex intensity, and Couette correction.

It should be remarked that this work finds application in polymer processing, where the use of lubricants that migrate to the wall is common, which promotes slip. Recirculation are usually undesired in polymer processing unless some kind of mixing is needed. The presence of recirculating flows leads to the accumulation of polymer melt in particular regions (contractions and expansions), resulting in the degradation of the material due to its long exposure to high temperatures. This can compromise the quality of the final product and also increase the production time (resulting in extra costs) since there is the need to clean the machinery (the molten material gets clogged in the expansions and contractions) when a different material is going to be processed. Therefore, this work intends to be used as a qualitative guideline for technicians and engineers when using slip promoters.

Regarding the numerical work, in our Newtonian fluid flow calculations, there is no need for any direct relaxation of the slip velocity. Instead, we use an efficient procedure, proposed in the work of Ferrás *et al.*,[41–43] that calculates the slip velocity along an iterative process, adjusting the calculations depending on the proximity to the final solution. When convergence is eminent, the calculated slip velocity converges to the correct slip velocity, while far from the solution, the new procedure guarantees that the slip velocity is always smaller than the velocity at the center of the adjacent control volume, an important requirement for convergence.

In contrast to contraction flows,[42,44,45] it was possible to obtain convergence in these expansion flow calculations for high values of the Deborah number, where we found the complete suppression of recirculation for high slip coefficients, and that wall slip reduces both the fluid expansion in the outer channel and the critical Deborah number.[46]

The remainder of this paper is organized as follows: Sec. II presents the governing equations together with the linear and nonlinear Navier slip boundary conditions used. In Sec. III, we briefly describe the solver used to couple velocity, pressure, and the slip boundary condition, and we also present the geometry and the

characteristics of the flow. In Sec. IV A, the results for the Newtonian fluid case ($De = 0$) are presented and discussed, while the viscoelastic flows are presented in Sec. IV B. The main conclusions of this paper are presented in Sec. V.

II. GOVERNING EQUATIONS

The governing equations for the laminar and incompressible fluid flows are the mass conservation,

$$\nabla \cdot \mathbf{u} = 0, \tag{1}$$

and momentum balance,

$$\rho \frac{\partial \mathbf{u}}{\partial t} + \rho \nabla \cdot (\mathbf{uu}) = -\nabla p + \nabla \cdot \boldsymbol{\tau}. \tag{2}$$

Additionally, an appropriate constitutive relation for the extra-stress tensor $\boldsymbol{\tau}$ is used. The stress tensor ($\boldsymbol{\tau} = \boldsymbol{\tau}_s + \boldsymbol{\tau}_p$) is split into a Newtonian solvent contribution, $\boldsymbol{\tau}_s$,

$$\boldsymbol{\tau}_s = \eta_s \left(\nabla \mathbf{u} + (\nabla \mathbf{u})^T \right), \tag{3}$$

and a polymer contribution, $\boldsymbol{\tau}_p$ (for a Newtonian fluid, $\boldsymbol{\tau} = \boldsymbol{\tau}_s$), here described by a widely used constitutive model, the simplified Phan–Thien–Tanner (sPTT),[6]

$$f(\mathrm{tr}\,\boldsymbol{\tau}_p)\boldsymbol{\tau}_p + \lambda \left(\frac{\partial \boldsymbol{\tau}_p}{\partial t} + \mathbf{u} \cdot \nabla \boldsymbol{\tau}_p - \left[(\nabla \mathbf{u})^T \cdot \boldsymbol{\tau}_p + \boldsymbol{\tau}_p \cdot \nabla \mathbf{u} \right] \right) = \eta_p \left(\nabla \mathbf{u} + (\nabla \mathbf{u})^T \right). \tag{4}$$

For the function $f(\mathrm{tr}\,\boldsymbol{\tau}_p)$, we use its linear form,

$$f(\mathrm{tr}\,\boldsymbol{\tau}_p) = 1 + \frac{\varepsilon \lambda}{\eta_p} \mathrm{tr}(\boldsymbol{\tau}_p). \tag{5}$$

These equations can be written in dimensionless form by considering the new variables $\mathbf{u}' = \mathbf{u}/U_1$, $t' = t/(H_1/U_1)$, $\mathbf{x}' = \mathbf{x}/H_1$, $p' = p/(\rho U^2)$, and $\boldsymbol{\tau}' = \boldsymbol{\tau} H_1/(\eta_0 U_1)$,

$$\nabla' \cdot \mathbf{u}' = 0, \tag{6}$$

$$\frac{\partial \mathbf{u}'}{\partial t'} + \nabla' \cdot (\mathbf{u}'\mathbf{u}') = -\nabla' p' + \frac{1}{Re} \nabla' \cdot \boldsymbol{\tau}', \tag{7}$$

$$f(\mathrm{tr}\boldsymbol{\tau}_p')\boldsymbol{\tau}_p' + De \left(\frac{\partial \boldsymbol{\tau}_p'}{\partial t'} + \mathbf{u}' \cdot \nabla' \boldsymbol{\tau}_p' - \left[(\nabla' \mathbf{u}')^T \cdot \boldsymbol{\tau}_p' + \boldsymbol{\tau}_p' \cdot \nabla' \mathbf{u}' \right] \right) = (1-\beta) \left(\nabla' \mathbf{u}' + (\nabla' \mathbf{u}')^T \right), \tag{8}$$

$$f(\mathrm{tr}\boldsymbol{\tau}_p') = 1 + \frac{\varepsilon De}{1-\beta} \mathrm{tr}(\boldsymbol{\tau}_p'). \tag{9}$$

In Eqs. (1)–(9), $\mathbf{u}$ is the velocity vector, p is the pressure, $\boldsymbol{\tau}$ is the extra-stress tensor, η_s and η_p are the solvent and zero shear polymer viscosity contributions, respectively, λ is the relaxation time, ε is the extensibility parameter of the PTT fluid, $\beta = \frac{\eta_s}{\eta_0} = \frac{\eta_s}{\eta_s + \eta_p}$ is the viscosity ratio, and $\mathbf{x}$ is the space vector.

In order to consider the possibility of slip at the boundary wall, we use the linear ($m = 1$)[47] and nonlinear Navier slip boundary conditions ($m \neq 1$),[48]

$$\|\mathbf{u}_{ws}\| = k \|\boldsymbol{\tau}_w\|^m, \tag{10}$$

where the parameter $k \geq 0$ is the slip coefficient (it will depend on the material employed and on the flow conditions and is normally calculated based on a fit to experimental data) that allows us to control the amount of slip. In Eq. (10), the slip velocity vector $\mathbf{u}_{ws}$ (the subscript "ws" stands for "wall slip") and the tangent stress $\boldsymbol{\tau}_w$ (the subscript "w" stands for "wall") are tangent to the walls, and the double bars indicate vector magnitude.

III. NUMERICAL PROCEDURE AND CASE STUDIES

The system of equations, Eqs. (1)–(10), is solved with a finite volume method code (see Ref. 50), using the SIMPLEC method of Van Doormaal and Raithby[49] to compute velocity and pressure fields. For the implementation of the slip boundary conditions, we use two slightly different methods, one for the linear Navier slip law and the other for the nonlinear Navier slip law.[41–43] For Newtonian or generalized Newtonian fluids, the flow near the wall is viscometric so that the magnitude of the tangent stress at the wall can be approximated by[51]

$$\|\boldsymbol{\tau}_w\| = \eta_w \left| \frac{\mathrm{d}u_t}{\mathrm{d}n} \right|_w, \tag{11}$$

where $\frac{\mathrm{d}u_t}{\mathrm{d}n}$ is the velocity gradient in the wall normal direction, u_t is the velocity component parallel to the wall, and η_w is the shear viscosity evaluated at the local wall shear rate.

Assuming Cartesian coordinates, orthogonal meshes, and a one-sided first order approximation for the velocity derivative, the relationship between the slip velocity and the tangent stress vector can be written as

$$u_{ws} = k \left(\eta_w \frac{|u_{\mathrm{P,t}} - u_{ws}|}{\delta n} \right)^{m-1} \frac{\eta_w (u_{\mathrm{P,t}} - u_{ws})}{\delta n}, \tag{12}$$

where u_{ws} is the slip velocity, parallel to the wall, $u_{\mathrm{P,t}}$ is the component of the velocity vector, at the center of the adjacent computational cell and parallel to the wall, and δn is the distance between the center (P) of the adjacent cell and the wall boundary (see Fig. 2).

Regarding the implementation of the slip boundary condition, two different linearizations were used, depending on the numerical value of the exponent m. For $m = 1$, we assume that only the slip

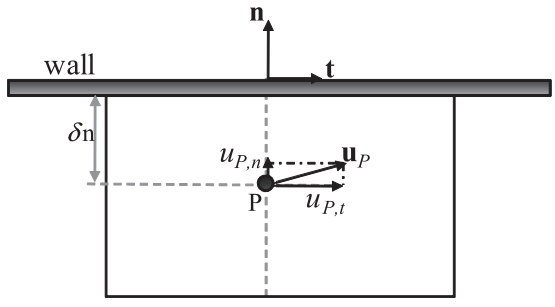

FIG. 2. Schematic of a computational cell.

velocity variable comes from the present iteration/time step, i, thus leading to the following relationship between u^i_{ws} and $u^{i-1}_{P,t}$:

$$u^i_{ws} = k\left(-\eta^{i-1}_w \frac{(u^i_{ws} - u^{i-1}_{P,t})}{\delta n}\right) \Rightarrow u^i_{ws} = \frac{a}{a+1} u^{i-1}_{P,t} \text{ with } a = k\frac{\eta^{i-1}_w}{\delta n}. \quad (13)$$

For $m \neq 1$, the discretized form of the nonlinear Navier slip law can be linearized assuming that only the slip velocity of the linear part comes from the present iteration (i) as

$$u^i_{ws} = k\left(\frac{\eta^{i-1}_w}{\delta n}\right)^m \left(u^{i-1}_{P,t} - u^i_{ws}\right)\left|u^{i-1}_{P,t} - u^{i-1}_{ws}\right|^{m-1}, \quad (14)$$

leading to

$$u^i_{ws} = \frac{l}{1+l} u^{i-1}_{P,t} \text{ with } l = k\left(\frac{\eta^{i-1}_w}{\delta n}\right)^m \left|u^{i-1}_{P,t} - u^{i-1}_{ws}\right|^{m-1}. \quad (15)$$

The main feature of this method is the guarantee that the slip velocity is always smaller in magnitude than the velocity at the center of the adjacent computational cell, a necessary condition for convergence. To solve the system of equations, we use the following iterative procedure:[41,42]

(1) Set the boundary conditions, the initial velocity, and pressure fields.
(2) Solve the constitutive equations for the non-Newtonian model.
(3) Compute the slip velocity with the discretized slip model, Eq. (13) or (15).
(4) Solve the momentum balance equation.
(5) Solve the pressure correction equation.
(6) Correct velocity and pressure fields.
(7) Check for convergence, based on the system of equation residuals.
(8) If convergence is not achieved, proceed to step 2.

The numerical method used to calculate the slip velocity for $De > 0$ is described in detail in Ferrás *et al.*[42] Here, the major difference to the earlier method is the use of linear extrapolation to obtain the stress at the wall.

In this work, we are interested only in the stationary solution, so the time evolution is used only for numerical relaxation purposes. Each time step represents one iteration i. With this method, there is no need for the explicit use of relaxation of the slip velocity and the computations are stable.

It should be remarked that all the numerical implementations were validated against the results obtained in Ferrás *et al.*[41–43] The numerical code is practically the same, and we have compared the fully developed solutions in both narrow and large channels against the analytical solutions for fully developed slip flows.

A schematic of the 1:4 expansion geometry is given in Fig. 1. We assume that the flow is two-dimensional and impose symmetry at the centerline $y = 0$. At the inlet, a uniform velocity profile U_1 is imposed together with null extra-stress components. To perform the numerical simulations for the expansion flow, we built three different meshes ME1, ME2, and ME3 (cf. Fig. 3), with consistent consecutive refinement, in the sense that the number of cells was doubled in each direction, with mesh spacing being approximately halved from mesh ME1 to ME2 and from ME2 to ME3. In this way, we can easily estimate the accuracy of the numerical predictions by using Richardson's extrapolation technique.[52,53]

	ME1		ME2		ME3	
Zone	nx	ny	nx	ny	nx	ny
1	15	36	30	72	60	144
2	87	36	174	72	348	144
3	87	36	174	72	348	144
4	87	47	174	94	348	188
5	87	18	174	36	348	72
6	15	36	30	72	60	144
7	15	47	30	94	60	188
8	15	18	30	36	60	72
NC	13974		55896		223584	
$\Delta x_{min}/d$	0.01		0.005		0.0025	

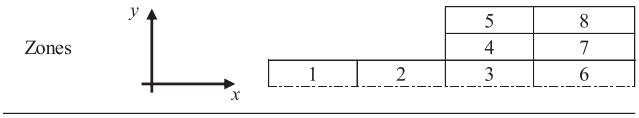

FIG. 3. Characteristics of meshes ME1, ME2, and ME3, and illustration of the blocks used.

To generate the meshes, the computational domain was divided into eight blocks and the notations n_x and n_y are used to represent the number of cells in the x and y directions, respectively. The mesh data are provided in Fig. 3.

We performed a large number of simulations, mostly because of the wide range of slip coefficients used (for each De, we typically used 15 different slip coefficients), to capture the influence of slip velocity on the flow behavior. Most results shown here were obtained with mesh ME2. Mesh ME3 was also used to test the accuracy of the method but only for a limited number of simulations because of the large computation times required.

The simulations were performed for the sPTT model at a constant $Re = \rho U_1 H_1/\eta_0 = 0.001$, and a varying $De = \lambda U_1/H_1$ ($De = 0$, 1, 2, 3, 4, 5, 10, 50, and 100) with $\varepsilon = 0.25$ and viscosity ratio $\beta = \frac{\eta_s}{\eta_0} = \frac{\eta_s}{\eta_s+\eta_p} = \frac{1}{9}$. Several values of the normalized slip coefficient, $k^*_l = \frac{k\eta_0}{H_1}$ (assuming that $m = 1$), were used.

The numerical results were analyzed in terms of the vortex sizes $X_R = x_R/H_1$ and $Y_R = y_R/H_1$ (cf. Fig. 1) and vortex intensity, the latter defined here as the recirculating flow rate inside the vortex normalized by the flow rate in the entrance channel,

$$\Psi_R = \frac{\psi_R - U_1 H_1}{U_1 H_1} \times 10^3, \quad (16)$$

where ψ_R is the streamfunction value at the vortex center (we assume that $\psi_R = 0$ at the centerline, $y = 0$). In addition, we also provide the Couette correction given by

$$C = \frac{\Delta p - \Delta p_{1FD} - \Delta p_{2FD}}{2\tau_w}, \quad (17)$$

where Δp represents the pressure drop between two points located far away from the expansion plane, one upstream and another downstream, Δp_{1FD} and Δp_{2FD} are the pressure drops for the fully

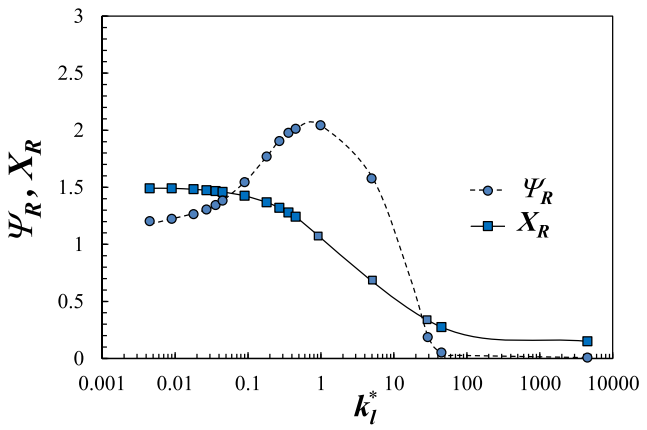

FIG. 4. Variation of the dimensionless vortex size, X_R, and vortex intensity, Ψ_R, with k_l^* for a Newtonian fluid (De = 0). The lines are a guide to the eye.

developed flows in the entry and exit channels (considering the same points used for Δp), with half widths H_1 and H_2, respectively, and τ_w is the wall shear stress encompassing both the solvent and polymer contributions for the fully developed flow at the entrance channel.

Additional plots are also presented, such as the variations of velocity and stresses along the centerline, and streamline maps, together with the characterization of the flow on the basis of the flow type parameter, ξ, defined as[54]

$$\xi = \frac{|\mathbf{D}| - |\mathbf{\Omega}|}{|\mathbf{D}| + |\mathbf{\Omega}|}, \tag{18}$$

where $|\mathbf{D}|$ and $|\mathbf{\Omega}|$ represent the magnitudes of the rate of deformation and vorticity tensors, respectively,

$$\mathbf{D} = \frac{1}{2}\left[\nabla\mathbf{u} + (\nabla\mathbf{u})^{\mathrm{T}}\right], \quad \mathbf{\Omega} = \frac{1}{2}\left[\nabla\mathbf{u} - (\nabla\mathbf{u})^{\mathrm{T}}\right], \tag{19}$$

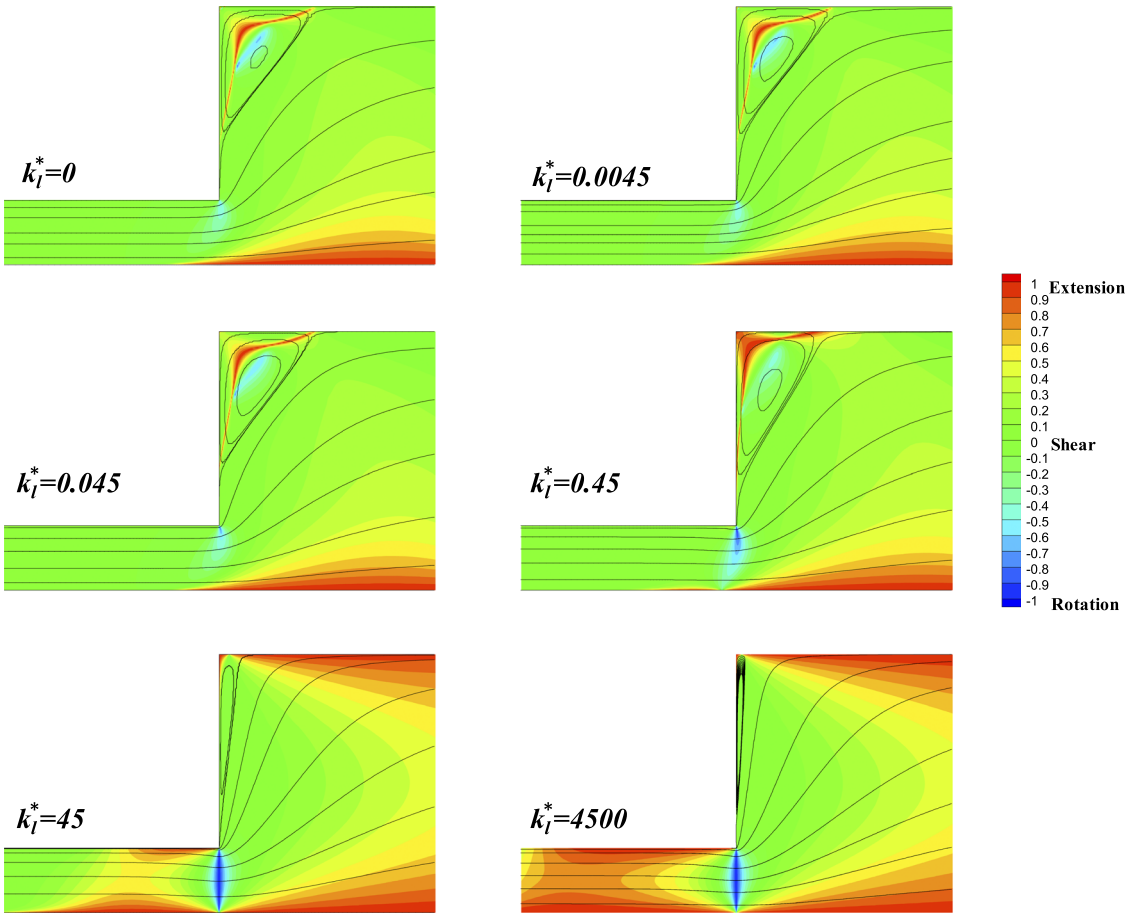

FIG. 5. Streamlines and flow type ξ for a Newtonian fluid (De = 0) and different values of the slip coefficient k_l^*, considering the linear Navier slip law.

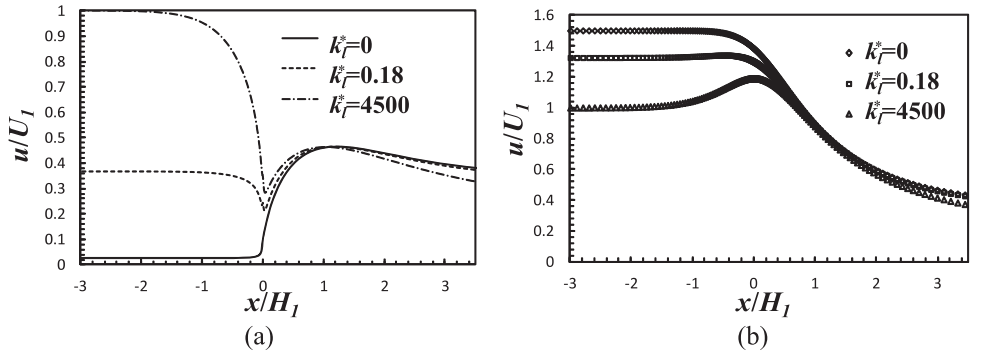

FIG. 6. Dimensionless axial velocity profiles along the channel for a Newtonian fluid (*De* = 0). (a) y/H_1 = 0.99 and (b) y/H_1 = 0.

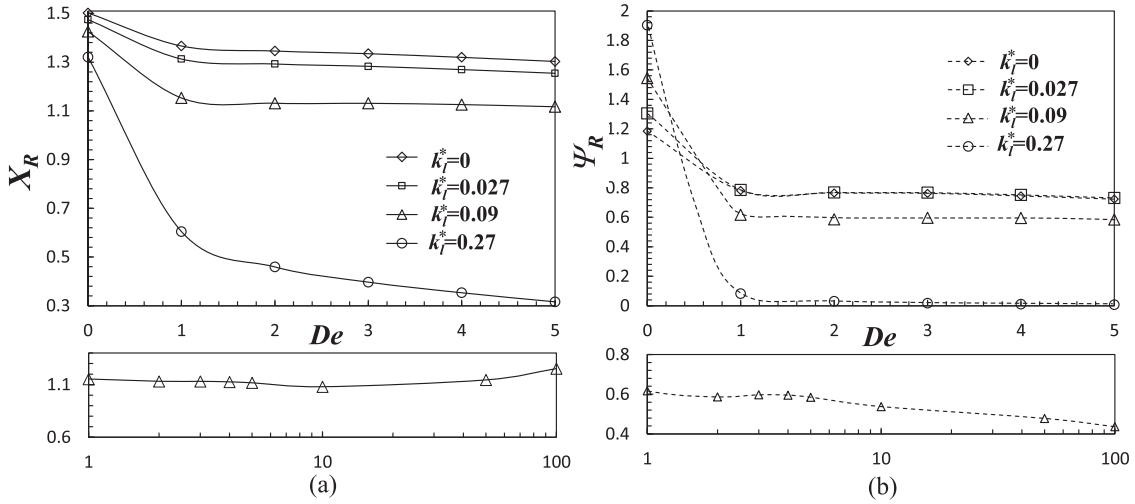

FIG. 7. Variation of (a) vortex dimension, X_R, and (b) vortex intensity, Ψ_R, with *De*, for different values of k_l^* (the lines are just a guide to the eye).

TABLE I. Variation of vortex dimension X_R with the slip coefficient k_l^* for *De* = 1.

k_l^*	ME1	ME2	ME3	Ext. X_R	Error (%)
0	1.3635	1.3665	1.3676	1.3681	0.04
0.0045		1.3586			
0.009	1.3475	1.3497	1.3509	1.3522	0.09
0.018		1.3319			
0.027		1.3136			
0.036	1.2879	1.2910	1.2931	1.2968	0.28
0.045		1.2704			
0.09		1.1627			
0.18	0.8731	0.8991			
0.27		0.6247			
0.36		0.2756			
0.45	0	0			
45	0	0			
4500	0	0			

TABLE II. Variation of the vortex intensity Ψ_R with the slip coefficient k_l^* for *De* = 1.

k_l^*	ME1	ME2	ME3	Ext. Ψ_R	Error (%)
0	0.7785	0.7813	0.7817	0.7817	0.008
0.0045		0.7880			
0.009	0.7881	0.7909	0.7920	0.7926	0.079
0.018		0.7932			
0.027		0.7856			
0.036	0.7697	0.7777	0.7795	0.7800	0.064
0.045		0.7572			
0.09		0.6269			
0.18	0.2750	0.2946			
0.27		0.0830			
0.36		0.0045			
0.45	0	0			
45	0	0			
4500	0	0			

which are given by

$$|\mathbf{D}| = \sqrt{\frac{1}{2}\left(\mathbf{D} : \mathbf{D}^{\mathrm{T}}\right)} = \sqrt{\frac{1}{2}\sum_i \sum_j D_{ij}^2},$$
$$|\mathbf{\Omega}| = \sqrt{\frac{1}{2}\left(\mathbf{\Omega} : \mathbf{\Omega}^{\mathrm{T}}\right)} = \sqrt{\frac{1}{2}\sum_i \sum_j \Omega_{ij}^2}. \tag{20}$$

The flow type parameter varies from −1, which corresponds to solid-like rotation, up to 1, for pure extensional flow. Pure shear flow is characterized by $\xi = 0$.

IV. RESULTS AND DISCUSSION

A. Newtonian fluids

For Newtonian fluids ($De = 0$), we observe in Fig. 4 that the axial vortex dimension, X_R, decreases with the slip coefficient, k_l^*, while the vortex intensity, Ψ_R, is non-monotonic with k_l^*. As slip increases above $k_l^* = 0.45$, the vortex intensity is now strongly reduced but the vortex itself does not vanish; it just becomes less elongated and more parallel to the expansion plane wall (cf. Fig. 5). This is seen as a strong reduction in X_R and Ψ_R.

This behavior is somehow different from that observed for viscoelastic fluids (see Sec. IV B), where the vortex vanishes for high slip velocity. We can also observe, in Fig. 5, that the region of shear flow near the channel walls for no-slip velocity ($k_l^* = 0$) and low slip coefficients ($k_l^* = 0.0045$ and $k_l^* = 0.045$) evolves for $k_l^* \geq 0.45$ into regions of extensional flow.

We also plotted the variation of the dimensionless streamwise velocity component along the channel at $y/H_1 = 0.99$ [Fig. 6(a)] and $y/H_1 = 0$ [Fig. 6(b)]. As the slip coefficient increases, especially for high slip coefficients, there is an abrupt change in the velocity profile near the extension plane, especially near the wall ($y/H_1 = 0.99$), because increasing slip turns the velocity profile

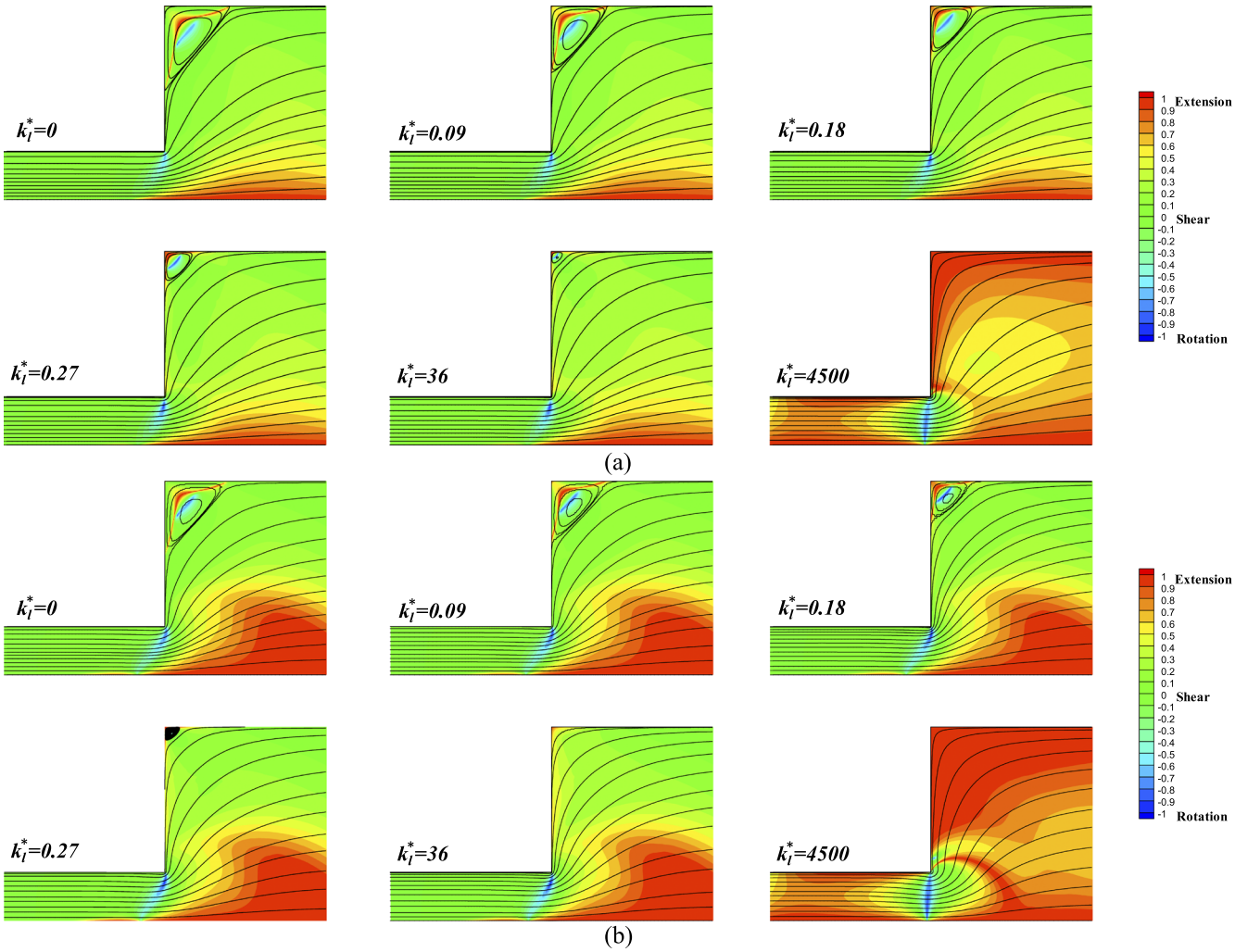

FIG. 8. Streamlines and flow type, ξ, for different values of the slip coefficient k_l^*. (a) $De = 1$ and (b) $De = 5$.

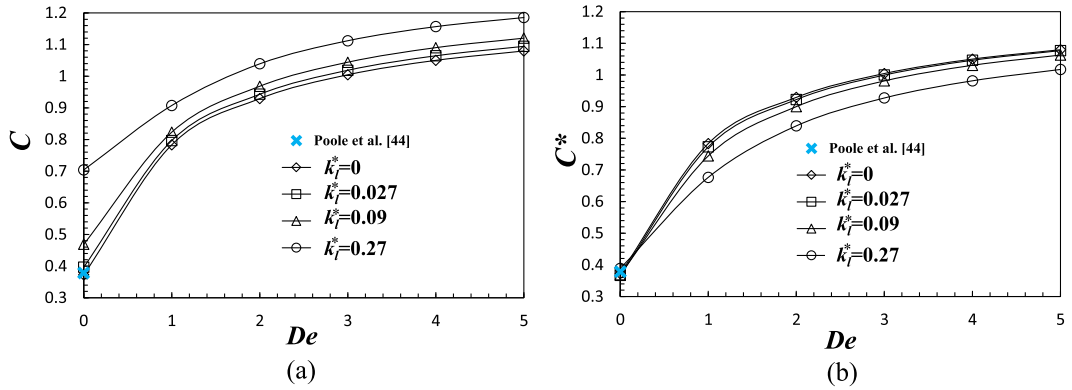

FIG. 9. Couette corrections as function of *De*. (a) *C* and (b) *C**.

progressively into a plug in the entry channel and then drastically reduces due to the expansion. It then increases downstream of the expansion zone, creating sharp peaks in the velocity gradient. As shown in Fig. 6(b), on approaching the expansion plane along the centerline ($y/H_1 = 0$), the fluid moves away from the wall and toward the center of the channel. Then again it goes away from the center as it fills the wider channel. We can observe in Fig. 5 that there is an actual contraction of the flow on approaching the expansion plane, and that is why, along the centerline we observe a local maximum in *u*.

B. Viscoelastic fluids

1. Effect of elasticity and slip

In addition to the Newtonian fluid limit ($De = 0$), the 1:4 expansion flow was also analyzed for De = 1, 2, 3, 4, and 5 over a wide range of slip coefficients and for De = 10, 50, and 100 at two different slip coefficients due to the significant computational time needed to attain converged solutions.

Figure 7 shows the variation of X_R and Ψ_R with De for several slip coefficients, k_l^*. We observe that vortex size and intensity decrease with De and k_l^*, with the vortex vanishing for the highest values of the slip coefficient as elasticity increases. Some of these results can also be seen in Tables I and II (for De = 1), where the accuracy of the results was assessed with Richardson's extrapolation technique for three different values of the slip coefficient. The variations of X_R and Ψ_R for higher values of De are also shown for a constant slip coefficient $k_l^* = 0.09$. We observe that Ψ_R decreases with De while X_R decreases with both k^* and De, except at very high De, where an increase is observed. These findings are in agreement with the conclusions of Poole *et al.*[7] The non-monotonic behavior at large De is a consequence of the large time it takes for the elastic stresses to relax or build up as compared to the flow transit time, so the flow tends to a viscous behavior when it negotiates the expansion region.

In Fig. 8, we show the streamlines superimposed on contour plots of ξ for different values of the slip coefficient and two different values of the Deborah number, De = 1 and 5. Contrarily to the Newtonian case, the vortex totally disappears with the

TABLE III. Variation of the Couette correction, *C*, with k_l^* for De = 1.

k_l^*	ME1	ME2	ME3	Ext. *C*	Error (%)
0	0.7851	0.7833	0.7826	0.7822	0.046
0.0045		0.7859			
0.009	0.7907	0.7883	0.7874	0.7867	0.084
0.018		0.7927			
0.027		0.7967			
0.036	0.8104	0.8006	0.7991	0.7989	0.034
0.045		0.8056			
0.09		0.8230			
0.18	0.8669	0.8627			
0.27		0.9075			
0.36		0.9574			
0.45	1.0152	1.0123			
45	47.246	47.456			
4500	4718.2	4736.2			

TABLE IV. Variation of the Couette correction, *C**, with k_l^* for De = 1.

k_l^*	ME1	ME2	ME3	Ext. *C**	Error (%)
0	0.7851	0.7833	0.7826	0.7822	0.046
0.0045		0.7820			
0.009	0.7827	0.7804	0.7796	0.7867	0.084
0.018		0.7768			
0.027		0.7729			
0.036	0.7782	0.7688	0.7676	0.7674	0.026
0.045		0.7656			
0.09		0.7442			
0.18	0.7107	0.7072			
0.27		0.6767			
0.36		0.6518			
0.45	0.6334	0.6317			
45	0.5765	0.5747			
4500	0.5795	0.5778			

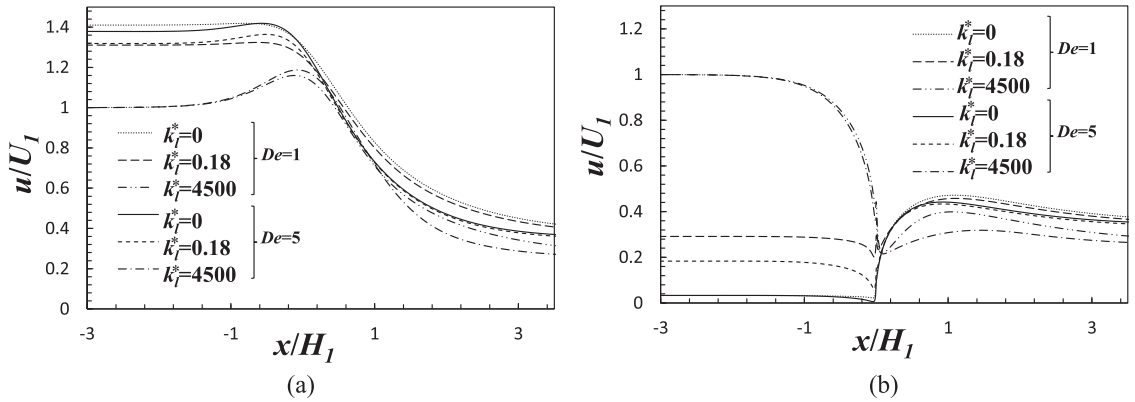

FIG. 10. Dimensionless axial velocity profiles along the channel for De = 1 and 5 and three different slip coefficients. (a) y/H_1 = 0 and (b) y/H_1 = 0.99.

increase in the slip velocity, and considerable changes in the vortex dimensions and shape appear first (for lower slip coefficients) for the viscoelastic case, especially for high Deborah numbers (De = 5). Note also that for De = 5, we obtain a wider region of extensional flow near the centerplane than at lower De, which can be justified by the higher relaxation time of the fluid that delays its deceleration in the expansion region, thus increasing the area where the flow is extensionally dominant. In contrast, the vortex suppression due to flow elasticity may be the consequence of the development of normal stresses in the transverse direction in the upstream channel. Once the upstream wall disappears, a strong normal stress gradient enhances flow in the transverse direction as a kind of swell effect. The overall conclusion, based on these figures, is that the vortex dimensions decrease with the increase in elasticity and slip intensity.

Regarding the Couette correction, C, Figs. 9(a) and 9(b) show the variation of C and C^* with De for different values of the slip coefficient. C^* represents the Couette correction normalized with the wall tangent stress, τ_w, obtained for the case of no-slip velocity at the walls. This normalization is used because when k_l^* is very large, the actual value of τ_w vanishes, leading to very large values of C (C is normalized with the corresponding real wall stress). For a Newtonian fluid, our results match those of Poole *et al.*[55] In Tables III and IV, we can also observe the Couette corrections C and C^* obtained for different slip coefficients at De = 1. For the viscoelastic fluids, we can observe that both C and C^* increase with De, as also

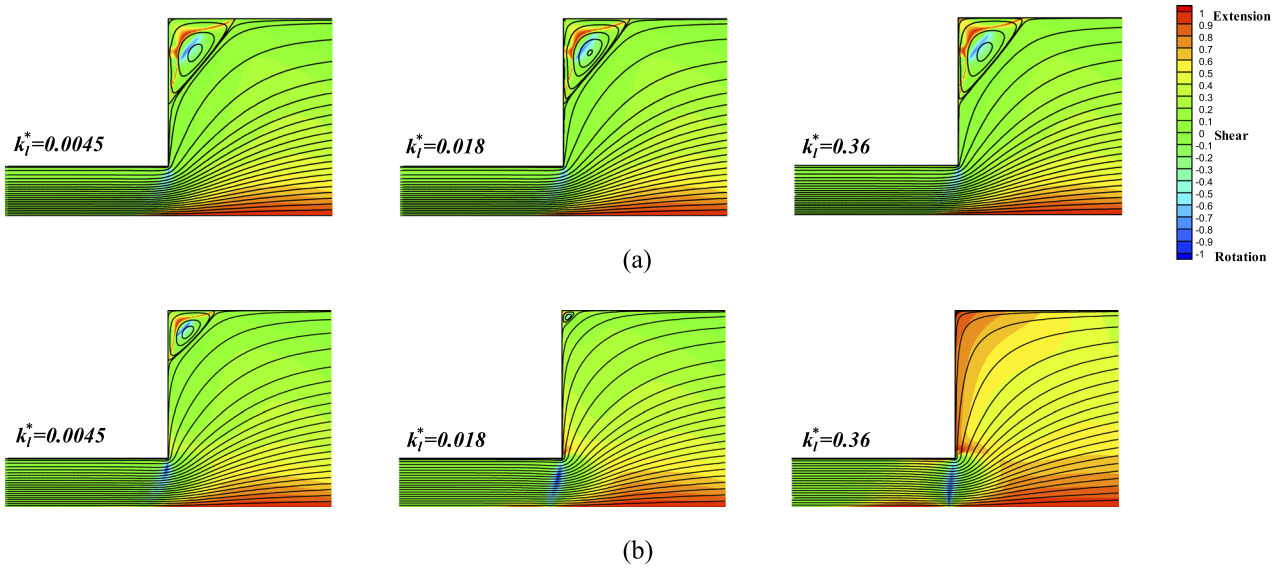

FIG. 11. Streamlines and flow type, ξ, for different values of the slip coefficient k_l^* for a constant De = 1 and two different slip exponents: (a) m = 0.5 and (b) m = 1.5.

observed in the data for the 1:3 expansion flow.[7] The Couette correction increases with k_l^* (a side effect of the chosen normalization), while the alternative Couette correction, C^*, decreases. This means that, contrarily to the behavior observed in data obtained by Ferrás *et al.*[42] for the 4:1 contraction flow, slip reduces C^*.

The dimensionless axial velocity profiles along the channel at two different positions, $y/H_1 = 0$ and $y/H_1 = 0.99$, are plotted for two different Deborah numbers, $De = 1$ and 5, in Fig. 10. For both De, the velocity near the wall increases with the slip coefficient, k_l^*, and higher velocities are attained for the smaller Deborah number, $De = 1$. This is more notorious for intermediate values of k_l^* and at the upstream channel. When the fluid is at the wider channel, the influence of the slip boundary condition is weakened by the larger distance between the centerplane and the wall and the changes between the velocity profiles for different De and k_l^* are less pronounced. This is a consequence of the unperturbed shape of the velocity profiles, which for the viscoelastic fluids are closer to uniform (plug-like) than the Newtonian profiles on account of the shear-thinning nature of the viscoelastic model selected. Hence, the higher the value of De, the weaker the variations in the velocity profile associated with imposing wall slip.

In order to evaluate the influence of the slip exponent, m, on the flow characteristics, we performed additional simulations for two different slip exponents with three different slip coefficients at a constant $De = 1$ (see Fig. 11). We can observe that for $m = 0.5$, the influence of $k^* = k\eta^m U^{m-1}/H_1^m$ on the flow is reduced, while for $m = 1.5$, the influence of k^* is enhanced. Note that for the case $k^* = 0.36$ and $m = 1.5$, we have an extensional flow region near the vortex corner that smears the vortex, while for the case $m = 0.5$, a rotational flow is still present indicating the existence of recirculation. This result is expected since the increase in the slip law exponent enhances slip.

V. CONCLUSIONS

Simulations were performed to evaluate the influence of the slip boundary condition on the 1:4 expansion flow of Newtonian and viscoelastic fluid flows. The presence of wall slip leads to a reduction in the vortex size and intensity, together with the reduction in the Couette correction C^*. The influence of the slip law exponent on the flow field was also investigated, and we found that a small slip exponent weakens the slip effect on the flow properties.

ACKNOWLEDGMENTS

A. M. Afonso acknowledges the support of CEFT (Centro de Estudos de Fenómenos de Transporte) and through Project Nos. PTDC/EMS-ENE/3362/2014 and POCI-01-0145-FEDER-016665—funded by FEDER funds through COMPETE2020—Programa Operacional Competitividade e Internacionalização (POCI) and by national funds through FCT—Fundação para a Ciência e a Tecnologia, I.P. A. M. Afonso, M. M. Alves, and F. T. Pinho are also grateful to FCT for funding through projects UIDB/00532/2020 and UIDP/00532/2020.

The research of L. L. Ferrás was partially financed by Portuguese Funds through FCT within the Project Nos. UIDB/00013/2020 and UIDP/00013/2020 and the scholarship Grant No. SFRH/BPD/100353/2014.

J. M. Nóbrega acknowledges the funding by FEDER funds through the COMPETE 2020 Program and National Funds through FCT—Portuguese Foundation for Science and Technology under the Project No. UID/05256/2020.

REFERENCES

[1] A. L. Halmos and D. V. Boger, "Flow of viscoelastic polymer solutions through an abrupt 2-to-1 expansion," Trans. Soc. Rheol. **20**, 253–264 (1976).
[2] A. L. Halmos, D. V. Boger, and A. Cabelli, "The behavior of a power-law fluid flowing through a sudden expansion. Part I. Numerical solution," AIChE J. **21**, 540–549 (1975).
[3] A. L. Halmos and D. V. Boger, "The behavior of a power-law fluid flowing through a sudden expansion. Part II. Experimental verification," AIChE J. **21**, 550–553 (1975).
[4] P. Townsend and K. Walters, "Expansion flows of non-Newtonian liquids," Chem. Eng. Sci. **49**, 748–763 (1994).
[5] A. Baloch, P. Townsend, and M. F. Webster, "On vortex development in viscoelastic expansion and contraction flows," J. Non-Newtonian Fluid Mech. **65**, 133–149 (1996).
[6] N. P. Thien and R. I. Tanner, "A new constitutive equation derived from network theory," J. Non-Newtonian Fluid Mech. **2**, 353–365 (1977).
[7] R. J. Poole, M. A. Alves, P. J. Oliveira, and F. T. Pinho, "Plane sudden expansion flows of viscoelastic liquids," J. Non-Newtonian Fluid Mech. **146**, 79–91 (2007).
[8] M. S. Darwish, J. R. Whiteman, and M. J. Bevis, "Numerical modelling of viscoelastic liquids using a finite-volume method," J. Non-Newtonian Fluid Mech. **45**, 311–337 (1992).
[9] K. A. Missirlis, D. Assimacopoulos, and E. Mitsoulis, "A finite volume approach in the simulation of viscoelastic expansion flows," J. Non-Newtonian Fluid Mech. **78**, 91–118 (1998).
[10] F. Durst, A. Melling, and J. H. Whitelaw, "Low Reynolds number flow over a plane symmetric sudden expansion," J. Fluid Mech. **64**, 111–128 (1974).
[11] W. Cherdron, F. Durst, and J. H. Whitelaw, "Asymmetric flows and instabilities in symmetric ducts with sudden expansions," J. Fluid Mech. **84**, 13–31 (1978).
[12] Y. Ouwa, M. Watanabe, and H. Asawo, "Flow visualization of a two-dimensional water jet in a rectangular channel," Jpn. J. Appl. Phys., Part 1 **20**, 243–247 (1981).
[13] E. M. Wahba, "Iterative solver and inflow boundary conditions for plane sudden expansion flows," Appl. Math. Modell. **31**, 2553–2563 (2007).
[14] G. N. Rocha, R. J. Poole, and P. J. Oliveira, "Bifurcation phenomena in viscoelastic flows through a symmetric 1:4 expansion," J. Non-Newtonian Fluid Mech. **141**, 1–17 (2007).
[15] R. J. Poole, M. P. Escudier, and P. J. Oliveira, "Laminar flow of a viscoelastic shear-thinning liquid through a plane sudden expansion preceded by a gradual contraction," Proc. R. Soc. London, Ser. A **461**, 3827 (2005).
[16] D. E. Abbott and S. J. Kline, "Experimental investigation of subsonic turbulent flow over single and double backward facing steps," J. Basic Eng. **84**, 317 (1962).
[17] M. P. Escudier, P. J. Oliveira, and R. J. Poole, "Turbulent flow through a plane sudden expansion of modest aspect ratio," Phys. Fluids **14**, 3641–3654 (2002).
[18] R. J. Poole and M. P. Escudier, "Turbulent flow of a viscoelastic shear-thinning liquid through a plane sudden expansion of modest aspect ratio," J. Non-Newtonian Fluid Mech. **112**, 1–26 (2003).
[19] R. J. Poole and M. P. Escudier, "Turbulent flow of viscoelastic liquids through an axisymmetric sudden expansion," J. Non-Newtonian Fluid Mech. **117**, 25–46 (2004).
[20] C. Dales, M. P. Escudier, and R. J. Poole, "Asymmetry in the turbulent flow of a viscoelastic liquid through an axisymmetric sudden expansion," J. Non-Newtonian Fluid Mech. **125**, 61–70 (2005).
[21] M. N. Azese, "Measurement and characterization of slippage and slip-law using a rigorous analysis in dynamics of oscillating rheometer: Newtonian fluid," Phys. Fluids **30**, 023103 (2018).
[22] M. Ebrahimi, V. K. Konaganti, and S. G. Hatzikiriakos, "Dynamic slip of polydisperse linear polymers using partitioned plate," Phys. Fluids **30**, 030601 (2018).

[23]M. N. Azese, "On the detection, measurement, and characterization of slip-velocity in Couette-rheology involving viscoelastic liquids," Phys. Fluids **31**, 023101 (2019).
[24]C. Chai and B. Song, "Stability of slip channel flow revisited," Phys. Fluids **31**, 084105 (2019).
[25]H. Fujioka and H.-H. Wei, "Letter: New boundary layer structures due to strong wall slippage," Phys. Fluids **30**, 121702 (2018).
[26]J. D. Evans, J. A. Cuminato, I. L. Palhares Junior, and C. M. Oishi, "Numerical study of the stress singularity in stick-slip flow of the Phan-Thien Tanner and Giesekus fluids," Phys. Fluids **31**, 093101 (2019).
[27]A. Shahbani-Zahiri, H. Hassanzadeh, M. M. Shahmardan, and M. Norouzi, "Investigation of pitchfork bifurcation phenomena effects on heat transfer of viscoelastic flow inside a symmetric sudden expansion," Phys. Fluids **29**, 113101 (2017).
[28]D. Izbassarov and M. Muradoglu, "A computational study of two-phase viscoelastic systems in a capillary tube with a sudden contraction/expansion," Phys. Fluids **28**, 012110 (2016).
[29]B. Lebon, M. Q. Nguyen, J. Peixinho, M. S. Shadloo, and A. Hadjadj, "A new mechanism for periodic bursting of the recirculation region in the flow through a sudden expansion in a circular pipe," Phys. Fluids **30**, 031701 (2018).
[30]R. Jamshidi, P. Angeli, and L. Mazzei, "On the closure problem of the effective stress in the Eulerian-Eulerian and mixture modeling approaches for the simulation of liquid-particle suspensions," Phys. Fluids **31**, 013302 (2019).
[31]A. V. Ramamurthy, "Wall slip in viscous fluids and influence of materials of construction," J. Rheol. **30**, 337–357 (1986).
[32]D. S. Kalika and M. M. Denn, "Wall slip and extrudate distortion in linear low density polyethylene," J. Rheol. **31**, 815–834 (1987).
[33]S. G. Hatzikiriakos and J. M. Dealy, "Wall slip of molten high density polyethylene. I. Sliding plate rheometer studies," J. Rheol. **35**, 497–523 (1991).
[34]S. G. Hatzikiriakos and J. M. Dealy, "Wall slip of molten high density polyethylene. II. Capillary rheometer studies," J. Rheol. **36**, 703–741 (1992).
[35]K. B. Migler, H. Hervet, and L. Leger, "Slip transition of a polymer melt under shear stress," Phys. Rev. Lett. **70**, 287–290 (1993).
[36]Y. Chen, D. M. Kalyon, and E. Bayramli, "Effects of surface roughness and the chemical structure of materials of construction on wall slip behavior of linear low density polyethylene in capillary flow," J. Appl. Polym. Sci. **50**, 1169–1177 (1993).
[37]K. M. Awati, Y. Park, E. Weisser, and M. E. Mackay, "Wall slip and shear stresses of polymer melts at high shear rates without pressure and viscous heating effects," J. Non-Newtonian Fluid Mech. **89**, 117–131 (2000).
[38]H. Münstedt, M. Schmidt, and E. Wassner, "Stick and slip phenomena during extrusion of polyethylene melts as investigated by laser-Doppler velocimetry," J. Rheol. **44**, 413–427 (2000).
[39]H. Gevgilili and D. M. Kalyon, "Step strain flow: Wall slip effects and other error sources," J. Rheol. **45**, 467–475 (2001).
[40]J. M. Dealy and S. Kim, "Gross melt fracture in extrusion," in *Polymer Processing Instabilities* (Marcel Dekker, NY, 2004), Chap. 7.
[41]L. L. Ferrás, J. M. Nóbrega, and F. T. Pinho, "Implementation of slip boundary conditions in the finite volume method: New techniques," Int. J. Numer. Methods Fluids **72**, 724–747 (2013).
[42]L. L. Ferrás, A. M. Afonso, M. A. Alves, J. M. Nóbrega, O. S. Carneiro, and F. T. Pinho, "Slip flows of Newtonian and viscoelastic fluids in a 4:1 contraction," J. Non-Newtonian Fluid Mech. **214**, 28–37 (2014).
[43]L. L. Ferrás, A. M. Afonso, J. M. Nóbrega, and F. T. Pinho, "A numerical and theoretical study on viscoelastic fluid slip flows," Phys. Fluids **29**, 053102 (2017).
[44]M. A. Alves, P. J. Oliveira, and F. T. Pinho, "Benchmark solutions for the flow of Oldroyd-B and PTT fluids in planar contractions," J. Non-Newtonian Fluid Mech. **110**, 45–75 (2003).
[45]A. M. Afonso, P. J. Oliveira, F. T. Pinho, and M. A. Alves, "Dynamics of high-Deborah-number entry flows—A numerical study," J. Fluid Mech. **677**, 272–304 (2011).
[46]N. Phan-Thien, "Influence of wall slip on extrudate swell: A boundary element investigation," J. Non-Newtonian Fluid Mech. **26**, 327–340 (1988).
[47]C. L. M. H. Navier, "Sur les lois du mouvement des fluids," Mem. Acad. R. Sci. Inst. Fr. **6**, 389–440 (1827).
[48]W. R. Schowalter, "The behavior of complex fluids at solid boundaries," J. Non-Newtonian Fluid Mech. **29**, 25–36 (1988).
[49]J. P. Van Doormaal and G. D. Raithby, "Enhancement of the SIMPLE method for predicting incompressible fluid flows," Numer. Heat Transfer **7**, 147–163 (1984).
[50]P. J. Oliveira, F. T. Pinho, and G. A. Pinto, "Numerical simulation of non-linear elastic flows with a general collocated finite-volume method," J. Non-Newtonian Fluid Mech. **79**, 1–43 (1998).
[51]J. Azaiez, R. Guénette, and A. Aït-Kadi, "Numerical simulation of viscoelastic flows through a planar contraction," J. Non-Newtonian Fluid Mech. **62**, 253–277 (1996).
[52]L. F. Richardson, "The approximate arithmetical solution by finite differences of physical problems including differential equations, with an application to the stresses in a masonry dam," Philos. Trans. R. Soc. London **210**, 307–357 (1911).
[53]L. F. Richardson and J. A. Gaunt, "The deferred approach to the limit," Philos. Trans. R. Soc. London **226**, 299–349 (1927).
[54]J. S. Lee, R. Dylla-Spears, N. P. Teclemariam, and S. J. Muller, "Microfluidic four-roll mill for all flow types," Appl. Phys. Lett. **90**, 074103 (2007).
[55]R. J. Poole, F. T. Pinho, M. A. Alves, and P. J. Oliveira, "The effect of expansion ratio for creeping flows of UCM fluids," J. Non-Newtonian Fluid Mech. **163**, 35–44 (2009).